Published in final edited form as:
ACS Appl Mater Interfaces. 2009 March 25; 1(3): 710–719. doi:10.1021/am8002318.

Tumor Targeting and Imaging in Live Animals with Functionalized Semiconductor Quantum Rods

Ken-Tye Yong[1], **Rui Hu**[1], **Indrajit Roy**[1], **Hong Ding**[1], **Lisa A. Vathy**[1], **Earl J. Bergey**[1], **Masamichi Mizuma**[2], **Anirban Maitra**[2], and **Paras N. Prasad**[1]

[1] Institute for Lasers, Photonics and Biophotonics, University at Buffalo, The State University of New York, Buffalo, New York 14260-4200

[2] Department of Pathology and Oncology, The Sol Goldman Pancreatic Cancer Research Center, CRB-2, Suite, 345, Johns Hopkins University School of Medicine, 1550 Orleans Street, Baltimore, Maryland 21231

Abstract

In this contribution, we demonstrate that highly luminescent CdSe/CdS/ZnS quantum rods (QRs) coated with PEGylated phospholipids and conjugated with cyclic RGD-peptide can be successfully used for tumor targeting and imaging in live animals. The design of these targeted luminescent probes involves encapsulating hydrophobic CdSe/CdS/ZnS QRs with PEGylated phospholipids, followed by conjugation of these PEGylated phospholipids to ligands that specifically target the tumor vasculature. *In vivo* optical imaging studies in nude mice bearing pancreatic cancer xenografts, both subcutaneous and orthotopic, indicate that the QR probes accumulate at tumor sites via the cyclic RGD-peptides on the QR surface binding to the$\alpha_V\beta_3$ integrins overexpressed in the tumor vasculature, following systemic injection. *In vivo* tumor detection studies showed no adverse effects even at a dose roughly 6.5 times higher than has been reported for *in vivo* imaging studies using QDs. Cytotoxicity studies indicated absence of any toxic effect in the cellular and tissue levels arising from functionalized QRs. These results demonstrate the vast potential of QRs as bright, photostable, and biocompatible luminescent probes for the early diagnosis of cancer.

Introduction

One-dimensional semiconductor nanostructures such as quantum wires (QWs)[1–7] and quantum rods (QRs)[8, 9] have been attracting significant interest over the last decade due to their tunable optical properties, which in turn give rise to applications in biomedical fields ranging from multiplex imaging to sensors[7, 10–17]. Recently, a wide array of methods in manipulating the shape and size of CdSe nanocrystals (NCs) have been reported[18]. For example, CdSe quantum rods were prepared by solution techniques using structure-directing agents[19], metallic nanoparticles[20], micellar templating techniques[21], etc[5, 22–25]. The controlled synthesis of NCs with various shapes is an important step in the development of ultrasensitive targeted probes for cancer research applications especially for early cancer detection[26, 27]. CdSe QRs have several advantages that make them potentially much better bioprobes in comparison to spherical quantum dots (QDs)[28]. These include larger absorption cross-section, and larger surface area per particle, which facilitates conjugation with multiple active molecules (e.g. probes for other imaging modalities, therapeutic molecules, biorecognition molecules for target specificity, etc)[29]. Their stokes-shift is strongly dependent on the aspect ratio (length/diameter) of the rod[30]. The emission of single QRs can be reversibly

pnprasad@buffalo.edu; kyong2@buffalo.edu.

switched on and off by externally applied electric fields. Also, it was reported that CdSe QRs emitted light that was linearly polarized along the c-axis of the crystallites and that the degree of polarization was dependent on the aspect ratio of the NCs31. Interestingly, despite these several advantages associated with QRs, investigations on their use in bioimaging only recently started, promoted by the advancement of well-controlled synthesis and surface functionalization approaches. Recently, Alivisatos' and our group have demonstrated live in vitro cancer cell imaging using CdSe/CdS/ZnS QRs as targeted luminescent probes32, 33. Both studies have showed the advantages of QRs as biocompatible targeted imaging probes. Alivisatos' group has demonstrated that QRs are brighter single molecule probes than QDs. Our group has shown that these QRs can be used for two-photon luminescence imaging of cancer cells in vitro with reduced photo-damage, as compared to UV-visible light excited single photon imaging.

Polyethyleneglycol grafted (PEGylated) phospholipids in aqueous media self-assemble into polymeric micelles with diameters generally smaller than 80 nm. Phospholipid micelles are more stable than detergent micelles and have very low critical micelle concentration (CMC) values (~10^{-6} M). Similar to detergent micelles, polymeric micelles solubilize "oil-like" particles by incorporating them into their hydrophobic core. More importantly, the outer surface of phospholipid micelles displays a dense layer of PEG that is non-immunogenic. This favors reduced capture and degradation by the reticuloendothelial system (RES), and yielded extended systemic circulation time, broad biodistribution, and lowered toxicity of the encapsulated nanoparticles. In addition, the PEG lipids can be further functionalized with specific reactive groups (e.g. carboxyl, amine, and maleimide) for conjugation purposes. Though micellar encapsulation of QDs has been demonstrated[34], we are not aware of any previous reports of producing high quality water-dispersible CdSe/CdS/ZnS QRs using phospholipid micelles for *in vivo* tumor targeting and imaging.

It is well known that new blood vessels (neovasculature) form around growing tumors in order to meet their demand of high nutrient supply, a process known as angiogenesis[35]. To achieve this, the endothelial cells surrounding tumor tissue organize themselves into capillaries that are attached to the extracellular matrix (ECM). Integrins such as $\alpha_V\beta_3$ are cell-surface receptors that anchor these endothelial cells to the ECM and transduce signals from the extracellular environment to the cell's interior. During angiogenesis, the $\alpha_V\beta_3$ integrins are known to be overexpressed on the surface of the endothelial cells surrounding tumor tissues. In addition, this integrin also plays a critical role in the invasion, metastasis, and proliferation of tumor[36]. Therefore, the $\alpha_V\beta_3$ integrin serves as an extremely potent target from the point of view of development of novel diagnostic and therapeutic probes that would specifically 'home in' on tumor sites *in vivo*. Of special interest is the triplet peptide Arg-Gly-Asp (RGD), which is known to specifically bind to the $\alpha_V\beta_3$ integrins overexpressed on the tumor endothelium, thus serving as an antagonist against vascular endothelial cell and tumor growth[37]. In addition to their potential role as a therapeutic molecule, RGD peptides modified with an imaging probe can also be used as a diagnostic tool to image $\alpha_V\beta_3$ integrin expression on developing tumors[38]. In this regard, QRs bioconjugated with RGD peptides, owing to their high luminescence, can potentially play a critical role towards the diagnosis of developing tumors *in vivo* via non-invasive optical imaging. In addition to pre-operative/therapeutic diagnosis, the QR labeled RGD peptides can also be used for image-guided surgery as they can delineate tumor margins from normal tissues during surgery. Thus, QR-labeled RGD peptides could be used as a new class of tumor (i.e. tumor angiogenesis) specific marker in cancer detection[39].

In this work, we aimed to first provide a "proof of principle" demonstration of *in vivo* tumor targeting and imaging using cyclic RGD (cRGD)-peptide-conjugated CdSe/CdS/ZnS QRs. These CdSe/CdS/ZnS QRs were first stably dispersed in aqueous solution by encapsulation within PEGylated and functionalized phospholipid micelles, a strategy which not only provided

PEG molecules on the QR surface for their enhanced colloidal stability in physiological circulation, but also active groups for an easy conjugation of synthetic cRGD peptides for tumor specific delivery. Following systemic injection of this QR formulation in mice bearing pancreatic cancer xenografts, we have demonstrated successful *in vivo* tumor labeling using whole body live animal optical imaging system, where the QR-targeted tumor can be easily distinguished from the background tissues (skin, hair, and food). This tumor imaging was demonstrated in mice bearing not only subcutaneously inoculated tumor xenografts, but also the more biologically relevant orthotopically implanted tumor xenografts. Furthermore, our biodistribution and cellular toxicity studies involving these highly luminescent QR-based probes in live animals indicated the absence of any observable toxicity, indicating the biocompatibility of these nanoprobes. These results underscore the potential of QRs as ultrasensitive and biocompatible optical probes for the early diagnosis of cancer and other diseases.

Experimental Section

Materials and Methods

A. Materials—Cadmium oxide, zinc acetate, sulfur, selenium, trioctylphosphine oxide (TOPO), trioctylphosphine (TOP), oleic acid, and HPLC water were purchased from Aldrich. Tetradecylphosphonic acid (TDPA) is a product of Alfa Aesar. RGD-peptides (PCI-3686-PI) were purchased from Peptides International, Inc. All chemicals were used as received. All solvents (hexane, toluene, and ethanol) were of reagent grade and were used without further purification.

B. Typical synthesis procedures

(i) Synthesis of CdSe quantum rods (QRs): The following protocol was adopted from our previous report[33] to obtain CdSe quantum rods. 1.6 mmol cadmium oxide, 3 mmol TDPA, and 3 g TOPO were loaded into a 100 ml three-necked flask. Next, the reaction mixture was slowly heated under an argon atmosphere to 290–300°C. After 10 to 15 minutes of heating, a clear homogeneous solution was obtained. The reaction mixture was maintained at 300°C for another 5 minutes, then 0.8 ml of 1 M TOP-Se was rapidly injected. The reaction was stopped after 2–3 minutes by removing the heating mantle. The QRs were separated from the surfactant solution by addition of ethanol and centrifugation. The reddish QR precipitate could be readily redispersed in various organic solvents (hexane, toluene, and chloroform).

(ii) Synthesis of CdSe/CdS/ZnS QRs with aspect ratio of ~4.6: The synthesis method of forming a CdS/ZnS graded shell on CdSe quantum rod was adapted from Manna et al[40]. CdSe quantum rod solution was prepared in advance by dissolving ~0.3 g of CdSe QRs in ~5 mL of toluene. Separately, 2 mmol of cadmium oxide, 4 mmol of zinc acetate, and 5.5 g of TOPO were dissolved in 10 mL of oleic acid. The reaction mixture was heated to 180°C for ~30 minutes under an argon flow, then the CdSe nanorod solution was injected slowly under stirring into the hot reaction mixture. The reaction mixture was held at 180°C, with a needle outlet that allowed the toluene to evaporate. After ~15 minutes of heating, the needle was removed, and the reaction temperature was raised to 210°C. Upon reaching the desire temperature, 2 mL of TOP-S was added drop wise into the reaction mixture. The reaction mixture was then held at ~210° for 10 to 15 minutes, then an aliquot was removed via syringe and was injected into a large volume of toluene at room temperature, thereby quenching any further growth of the QRs. The QRs were separated from the toluene solution by addition of ethanol and centrifugation.

C. Preparation of phopholipid-micelle encapsulated QRs—The as-prepared organic-dispersible QRs were separated from by addition of ethanol (volume ratio of QRs to ethanol

1:3) and centrifugation (12,000 rpm for 20 min). The precipitate was collected and dried in vacuum and re-dispersed in chloroform. Next, QRs dispersed in chloroform (~3 mg/mL), DSPE-mPEG (1,2-Diacyl-sn-Glycero-3-Phosphoethanolamine-N-[Methoxy(Polyethylene glycol)], Average MW 5000, Catalog Number: MPEG-DSPE-5000-1g, Laysan Bio, Inc) in chloroform solution (~10 mg/mL), and DSPE-PEG-Maleimide (1,2-Distearoyl-sn-Glycero-3-Phosphoethanolamine-N-[Maleimide(Polyethylene Glycol)], (Ammonium or sodium Salt), Average MW 3400, Catalog Number: DSPE-PEG-MAL-3400-1g, Laysan Bio, Inc) in chloroform solution (~10 mg/mL) were mixed together at a weight ratio of 1:4:0.5. The PEGylated phospholipids were purchased from Avanti polar lipids, Inc. and Laysan Bio Inc. Each mixture was gently stirred for 5 to 10 minutes. A Labconco rotory evaporator with a water bath of 25° was used to evaporate the organic solvent. The lipidic film, deposited on the reaction vial, was hydrated with 3 to 5 mL of HPLC water and subjected to ultrasonication for 10 to 20 minutes using a bath sonicator. The resulting dispersion was filtered through a 0.45 or 0.2 um membrane filter and kept at room temperature for further use. To remove the excess phospholipids from the QR dispersion, the micelle-encapsulated QRs were further purified using centrifugation at 10,000 rpm for 15 minutes. The QR precipitate was then re-dispersed in 1 to 2 mL of HPLC water (the water was filtered with 0.2 mm membrane filter).

D. Conjugation of micelle-encapsulated QRs with thiolated RGD—A 1 mL portion of micelle-encapsulated QR stock solution was mixed with 0.5 mL of 1.2 mg/mL thiolated RGD-peptide solution (molar ratio of Maleimide to RGD-peptide is 1:2) and gently stirred for 40 to 60 minutes. Next, the resulting bioconjugate dispersion was further purified using centrifugation at 10,000 rpm for 15 minutes. The QR precipitate was re-dispersed with 1 mL of HPLC water and kept at 4° for further use.

E. Spectral analysis of QRs—The absorption spectra of QRs were collected using a Shimadzu model 3101PC UV-Vis-NIR scanning spectrophotometer over a wavelength range from 400 to 900 nm. The samples were measured against chloroform (or water) as reference. The QR emission spectra were collected using a Fluorolog-3 Spectrofluorometer (Jobin Yvon; fluorescence spectra). Solution samples of QRs were filtered through a syringe filter (PTFE, pore size 450 nm), diluted to a concentration of about 0.01 g/L, and then loaded into a quartz cuvette for measurements. All the samples were dispersed in chloroform (or water) and loaded into a quartz cell for measurements. Fluorescence quantum yields (QYs) of the QR dispersions were determined by comparing the integrated emission from the nanocrystals to rhodamine 6G dye solutions of matched absorbance. Samples were diluted so that they were optically thin.

F. Particle size determination—High Resolution Transmission Electron Microscopy (HRTEM) images were obtained using a JEOL model JEM 2010 microscope at an acceleration voltage of 200 kV. The specimens were prepared by drop-coating the sample dispersion onto an amorphous carbon coated 300 mesh copper grid, which was placed on filter paper to absorb excess solvent. The size distribution and surface potential of micelle-encapsulated QRs were determined by dynamic light scattering (DLS) measurement with a Brookhaven Instruments 90Plus particle size analyzer, with a scattering angle of 90° For the potential measurement, a phase analysis light scattering (PALS) module was used.

G. Small animal imaging studies—Four to five weeks old nude female mice were purchased from Harlan Sprague Dawley Inc. The animal housing area was maintained at 24° C with a 12-hours light/dark cycle, and animals were fed ad libitum with water and standard laboratory chow. Animal experiments were performed in compliance with guidelines set by the University at Buffalo. All animals were acclimated to the animal facility for at least 48 hours prior to experimentation. Tumor model animals were generated by the subcutaneous inoculation (2–3 million cells/100 μL media) of human pancreatic cancer cell-line Panc-1

(ATCC NO: CRL-1469) in the shoulder of animals using a 1 mL syringe with 25G needle. After the tumor growth to a palpable size, the mice were administered with functionalized QRs in 1x PBS by tail vein injection and anesthetized with isoflurane at various time points post injection. The sedated animals were then imaged using the Maestro in vivo optical imaging system (CRI, Inc., Woburn, MA). For the tumor imaging studies, we used five mice each for the experimental and control groups.

H. Generation of orthotopic xenografts—Orthotopic pancreatic cancer xenografts were generated by surgical orthotopic implantation under the pancreatic capsule, as we have previously described[41, 42]. Imaging of the primary tumors was performed four weeks post-implantation.

Results and Discussion

The CdSe/CdS/ZnS QRs were prepared by solution phase synthesis as described in our previous studies, via growing a CdS/ZnS graded shell on CdSe rods in surfactant solution[33]. Oleic acid and TOPO were used to passivate the QR surfaces, thereby rendering them dispersible in chloroform. Phospholipid micelles were then used to enable the stable aqueous dispersion, generating a hydrophilic shell with PEG groups on QR surface (see Scheme 1). For *in vivo* tumor targeting and imaging studies, an optimized combination of maleimide-functionalized and non-functionalized phospholipid-PEGs were used to encapsulate the QRs and these encapsulated particles were further conjugated with thiolated cRGD (cyclo(Arg-Gly-Asp-D-Phe-Cys)) to act as biologically targeted luminescent probes.

In this study, the CdSe/CdS/ZnS QRs are coated with coordinating ligands such as hydrophobic moieties (TOPO and oleic acid), and a phospholipid-PEGs coating. The strong hydrophobic interactions between hydrophobic surfactants and the phospholipid hydrocarbon chains will produce two oil-like layers which interlock with each other and form a lamellar-like hydrophobic layer surrounding the rod surface that prevents the degradation even under biological fluids (see Scheme 1). As a result, after functionalizing with phospholipid-PEG molecules, the encapsulated QRs are protected in such a way that their optical properties (e.g., absorption spectra, emission spectra and quantum yield) remain unchanged in a broad range of pH (3 to 10) and temperature conditions (25 to 70°C)

Figure 1a and b present TEM images of the CdSe/CdS/ZnS QRs in organic media, which are approximately 20.5 nm in length and 4.5 nm in diameter. The lattice fringes of the CdSe/CdS/ZnS QRs are clearly shown in the inset, with fringe spacing of 3.5 A. Figure 1c and d show the phospholipid micelle-encapsulated QRs in aqueous media. A comparison of Figure 1a and 1b shows that the size and aspect ratio of the phospholipid micelle-encapsulated CdSe/CdS/ZnS QRs remain unchanged. This suggests that neither aggregation nor “ripening” of the QRs occurs during the phospholipid micelle encapsulation process. From the powder X-ray diffraction pattern of QRs, all of the diffraction peaks correspond to the wurtzite structure of CdSe. High-resolution transmission electron microscopy and powder X-ray diffraction confirmed that the growth axis of the rods was the *c*-axis of the wurtzite structure. The water dispersible, micelle encapsulated QRs were colloidally stable for more than three weeks at 4° C. Figure 2 shows the UV absorption and photoluminescence (PL) spectra from the monodispersed CdSe/CdS/ZnS QRs. The absorption spectrum features an excitonic peak around 649 nm. The PL spectrum of the monodispersed QRs shows a band edge emission at 658 nm. The PL quantum yield (QY) of the QRs is estimated to be ~50%. The inset shows the photograph of highly luminescent water-dispersible micelle-encapsulated QRs exposed by a handheld UV lamp.

It is favorable to reduce the hydrodynamic size of QR probes for better tumor targeting and imaging[43, 44]. We had initially replaced the hydrophobic moiety coating on the QR using thiolated PEG molecules to generate a PEGylated QR with a much smaller size. However, we have observed more than ~80% loss of their PL intensity immediately and further loss of the PL intensity was observed after one to two days of storage at room temperature. This strongly indicates that the QRs are very sensitive towards any ligand exchange process, thereby justifying our strategy of using phospholipid-PEG encapsulation approach to prevent the breakdown of QR.

Dynamic light scattering (DLS) was used to determine the hydrodynamic size and colloidal stability of the QRs dispersed in PBS (pH = 7.4). The DLS measurement shows that the engineered QR probes have a hydrodynamic radius of ~32 nm (see Figure 2b). Over the time range from 0 to 3 days, the effective radius varies by less than 20%, suggesting that their colloidal stability is not affected under physiological pH. It has been recently reported that PEGylated colloidal gold nanoparticles with hydrodynamic radius of 40–50 nm did not cause any difficulties for *in vivo* tumor imaging[45].

Prior to *in vivo* tumor imaging, body weight evaluation was performed on mice injected intravenously with the QRs in order to assess the signs of potential toxicity46. The body weight change is a useful indicative parameter for studying the acute toxic effects of administered nanoparticles in animals[47]. In this experiment, BALB/c mice were divided into 2 groups (5 mice per group), one group receiving 1 mg micelle-encapsulated QRs, and the other group did not receiving any injection. No significant differences in the average body weight between these two groups were observed for more than one week after the treatment of the micelle encapsulated-QRs. Also, physical evaluations of the QR treated mice did not indicate any changes in eating, drinking, exploratory behavior, and physical features (e.g. hair color). These preliminary studies indicate non-toxicity of these QRs in vivo, particularly in the short-term.

The maleimide functionalized phospholipid micelle-encapsulated QRs are conjugated with thiolated cRGD peptides for *in vivo* tumor targeting. These maleimide-functionalized QRs have roughly 200 maleimide groups on the surface of each QR. The maleimine groups on the particle surface were roughly estimated based on the assumptions as follows, we first assume a close-packed monolayer of the mixed surfactants (TOPO and oleic acid) on the surface of QR. In this case, the total of surfactants attached on a nanoparticle is $(4\pi r^2)/\alpha$, where r is the radius of the particle and α is the head area per molecule of the surfactant. Here, it is being assumed that the surfactants, TOPO and oleic acid are adsorbed to the QD surface to an equal extent, and their average head packing area is 21 $Å^2$ (α) as usually calculated for similar amphiphilic molecules. Also, we assume that each surfactant can only interact with one pegylated phospholipids molecule. Thus, one can finally determine the number of maleimide groups on the QD surface by including the final concentration fraction of DSPE-PEG-Maleimide into the calculation. In this study, a large excess of the thiolated cRGD were used for conjugation and we estimated that there are at least 150 to 200 cRGD peptides per QR based on the conjugation efficiency of the maleimide groups. The number of cRGD-peptides per rod is at least 3 to 4 times greater than that of the dot particle. To visualize synthesized QR bioconjugate, we again performed transmission electron microscopy on QR conjugated with cRGD. Specimens were prepared by drop-casting QR bioconjugates solution onto the TEM grid and the size of QR bioconjugates measured by TEM was similar to non-conjugated QRs (data not shown). The TEM analysis clearly indicated that the QR bioconjugates are monodispersed and do not show any sign of agglomeration or aggregation. The QR bioconjugates were colloidally and optically stable for one week in PBS buffer.

For *in vivo* whole body tumor imaging study, athymic nude mice bearing subcutaneous Panc-1 tumors (3–4 weeks post inoculation of 2–3 × 10^6 Panc-1 cells on the left shoulder, at a tumor

size of about ~0.5–0.9 cm^3) were injected (intravenously) with non-bioconjugated or cRGD-conjugated QRs (~1 mg of QR bioconjugates per animal, number of mice = 5). The mice were imaged at different time points starting from 1 to 24 hours post-injection using the Maestro *in vivo* imaging system (CRI, Inc., Woburn, MA; excitation filter: 445 – 490 nm, emission filter: 515 nm long-pass). The Maestro optical system consists of an optical head that includes a liquid crystal tunable filter (LCTF, with a bandwidth of 20 nm and a scanning wavelength range of 500–950 nm) with a custom-designed, spectrally optimized lens system that relays the image to a scientific-grade megapixel CCD. The CCD captured the images at each wavelength. The captured images (spectral cube, containing a spectrum at every pixel) can be loaded into the vendor software and analyzed. Spectra from the autofluorescence (from the skins, tissues, and food, coded green) and QR-associated luminescence signals (coded red) can be unmixed using the vendor software, as shown in Figure 3. In this study, the scanning wavelength range between 500 to 900 nm was used as recommended by the CRI instrument manual.

Figure 4 shows the *in vivo* luminescent imaging of Panc-1 tumor-bearing mice (in the left shoulder as pointed by white arrows) injected with ~1 mg of cRGD conjugated QR (panels a–f) and unconjugated QR (panels m–r), respectively. All images were acquired using the same instrumental conditions. It can be seen that within one hour of post injection, a strong luminescence signal was detected in the Panc-1 tumor. During the next 23 hours, a steady decrease in the tumor luminescent intensity in tumor-bearing mice treated with QR bioconjugates can be observed (see Figure 4, panels a–f), with almost no discernible signal even at 18 hours post-injection. Figure 5 shows the lateral view of the QR-cRGD treated Panc-1 tumor-bearing mice. These Figures corresponds to the panels a–f in Figure 4. In control experiments, no detectable luminescent signal was observed in the tumor for the non-bioconjugated QR injected mouse (number of mice = 5), at any time point post-injection (Figure 4, panels m–r,) indicating their poor tumor specificity. These results validate the high efficiency tumor targeting of cRGD-conjugated, as opposed to non-bioconjugated, QRs *in vivo*. It is worth mentioning that the QRs concentration used here is at least 6.5 times higher than that reported previously for *in vivo* imaging using other QDs[48]. This demonstrates the biocompatibility and negligible *in vivo* toxicity of the engineered QRs for *in vivo* applications.

To further prove that the engineered QRs can be used for early cancer detection, nude mice with 2 weeks post inoculation of $2–3 \times 10^6$ Panc-1 cells on their right shoulder (early stage of the tumor growth) were injected i.v. with the same QR-cRGD bioconjugates. Similar to that observed using bigger tumors (Figures 4 and 5), Figure 6 shows a strong luminescence signal emanating from the site of inoculation of tumor cells, thus demonstrating the ability of QR-cRGD bioconjugates to successfully enable targeted bioimaging of tumors during angiogenesis seen in early development of tumor.

To examine the distribution of functionalized QRs in tumor-bearing mice, they were sacrificed and major organs were removed for luminescence imaging after intravenously injected with QR bioconjugates for 72 hours. Luminescence images of heart, liver, spleen, lung, and kidney were obtained from tumor-bearing mouse after tail vein injection of functionalized QRs. As observed from the characteristic red luminescence of QRs, cRGD functionalized QRs uptake took place primarily in the liver and the spleen, with little or no QRs accumulation in the heart, the kidney and the lung. We noted that accumulation of QRs in liver and spleen were reduced with time. This pattern of *in vivo* organ distribution from small animals is similar to that of functionalized QD targeted probes previously reported[48, 49].

In addition to using mice bearing subcutaneous xenografts of pancreatic cancer, we have also carried out preliminary targeted bioimaging studies in mice bearing orthotopically implanted with human pancreatic cancer. In contrast to subcutaneous xenografts, orthotopic tumors, particularly those in the pancreas, simulate the pitfalls of *in vivo* targeted imaging in humans

due to their proximity to the hepatic and splenic fields, the latter being typical sources of artifactual fluorescence due to reticulo-endothelial uptake (see below). Demonstration of optimal imaging parameters in the orthotopic setting, thus, provides a considerably higher degree of confidence in the path towards clinical translation, not accorded by conventional subcutaneous tumors. It is also worth noting that the pattern of tumor angiogenesis in orthotopic primaries is more likely to recapitulate the cognate human disease, than the pattern arising in subcutaneous xenografts, a matter of not insignificant consideration when using a vascular targeted imaging strategy. Figure 8a shows the luminescence images of a dissected mouse bearing orthotopic pancreatic cancer xenografts, following 2 hours of intravenous injection of cRGD-QRs. From the figure, the successful targeting of the orthotopic tumor can be visualized by the characteristic red emission associated with the QRs. Figure 8c and b compares the images of the resected orthotopic tumors from mice injected with cRGD-targeted, as opposed to non-bioconjugated, QRs. The observation of red emission from the tumor of mouse receiving targeted QRs, but not from that of mouse receiving non-bioconjugated QRs, indicates that cRGD-conjugation is necessary for specifically targeting the QRs to orthotopic tumors *in vivo*.

For *in vivo* application, it is important to reduce QR uptake by the reticuloendothelial (RES) system. It is widely known in the field of targeted delivery that the functionalizing of an outer layer of polyethyleneglycol (PEG) on nanoparticles endows the nanoparticles with RES evading properties. This increases the circulation time of the nanoparticles in blood, thereby enhancing their ability to accumulate in solid tumors by passive diffusion, taking aid of the enhanced permeability and retentivity (EPR) effect. In this study, we have observed that by incorporating PEG into the QR bioconjugates, a reduced uptake in the liver, spleen, and bone marrows was observed upon comparing to other studies. However, without the cRGD peptide conjugated to the surface, little to no tumor accumulation of the PEG-phospholipid coated QRs was observed. Previous reports have mentioned that long PEG functionalized QDs may likely reduce the probability of QDs to target the tumor cells because of the substantially increased particle sizes. However, this scenario did not occur in our studies.

The above experiments successfully demonstrate that cRGD conjugated QRs can be used for targeted delivery and imaging of both subcutaneous and orthotopic tumors *in vivo*. To the best of our knowledge, this is the first successful demonstration of functionalized QRs for *in vivo* tumor targeting and imaging. The unique properties of the QRs can be combined with advances in targeted diagnostics and therapeutics thus paving the way for numerous novel biomedical applications involving QR-bioconjugates. Recently, we have reported the use of CdSe/CdS/ZnS QRs for multiplex labeling of live human cancer cells using single excitation source[50]. This technique was used to image human pancreatic cancer *in vitro*, by conjugating QRs with the monoclonal antibodies anti-claudin 4 or anti-mesothelin, which target the claudin-4 and mesothelin receptors overexpressed on pancreatic cancer. Therefore, it might be worth exploring the conjugation of different potential tumor targeting agents with QRs emitting in two or more colors for the simultaneous evaluation of the tumor specificity of these agents *in vivo*. We are currently in the process of investigating whether the different aspect ratio of QRs can give an extra degree of freedom to improve targeting efficiency and better *in vivo* imaging capability. In addition, multiple biomolecules can be conjugated to the large surface area of QR (per particle) to target multiple receptors on the tumor sites[51]. For example, a combination of monoclonal antibodies (anti-claudin 4 or anti- mesothelin) and RGD peptides can be used to modify the surface of micelle-encapsulated QRs for simultaneously *in vivo* labeling the tumor mass and the surrounding vasculature of pancreatic cancer, respectively.

In addition to UV-Vis range emitting QRs, QRs such as CdTe/CdSe/ZnS that emit at the NIR region may be a good alternative for *in vivo* tumor imaging especially in human studies because autofluorescence and light absorbance of biological specimens in the NIR regions are at their

minimal[52, 53]. Also, multimodality imaging of QR-based probes can be fabricated using solution phase synthesis method[47]. For example, QRs can be incorporated with paramagnetism and this multimodal QR will allow noninvasive tumor diagnosis using combined optical and MRI scans. The high QY, together with NIR-emitting luminescent wavelength and paramagnetism within one single multimodal QR probe makes it particularly attractive and promising for *in vivo* early cancer detection[54, 55], where the exact location and dimensions of tumor can be pinpointed precisely using concurrent MR and NIR luminescent imaging.

The low toxicity micelle-encapsulated QR probes developed here may provide a nanoplatform for early detection of human pancreatic cancer. Cancer of pancreas is the fourth leading cause of cancer-related mortality in the United States and accounts for more than 31,000 deaths each year[56]. The vast majority of patients present with locally advanced or distant metastatic disease, rendering the cancer inoperable. Current drug and radiation therapies have been ineffective in ameliorating the prognosis of this uniformly lethal disease. Therefore, in order to improve survival rate of pancreatic cancer patients, ultrasensitive imaging probes are needed for diagnosing pancreatic cancer at an early, and hence potentially curative, stage. We believe that current work will serve as an important milestone for future *in vivo* studies aimed at an early detection of pancreatic cancer, where better tumor locating efficiency can be achieved. Also, we envisioned that in those patients where early pancreatic cancer detection is achieved using QRs, more successful surgical intervention can be performed by optically guided surgery. This necessitates the removal of all cancerous area surrounding the tumor site without harming the normal tissue.

Conclusion

In summary, we have demonstrated that cRGD peptide-conjugated micelle-encapsulated QRs can be used as targeted probes for labeling cancer in vivo, using both subcutaneous and orthotopic models of pancreatic cancer bearing mouse. Since tumor vasculatures are over-expressesed with $\alpha_V\beta_3$ integrin, cRGD-QR bioconjugates can be served as a new class of anisotropic nanoparticle-based probes for early detecting and imaging cancer in vivo. More importantly, these probes are able to selectively target and image early tumor growth. The results reported here may aid in advancing the $\alpha_V\beta_3$ integrin-targeted luminescent imaging using anisotropic semiconductor nanoparticles and will have great potential for traceable drug delivery cancer therapy.

Acknowledgments

This study was supported by grants from the NCI (CA119397, CA119358, and CA104492) and the John R. Oishei Foundation. KTY is supported by the AACR-Pancreatic Cancer Action Network Fellowship for Pancreatic Cancer Research. KTY is grateful to the reviewers for their helpful comments.

References

1. Hull KL, Grebinski JW, Kosel TH, Kuno M. Chem Mater 2005;17(17):4416–4425.
2. Li C, Curreli M, Lin H, Lei B, Ishikawa FN, Datar R, Cote RJ, Thompson ME, Zhou C. J Am Chem Soc 2005;127(36):12484–12485. [PubMed: 16144384]
3. Morales AM, Lieber CM. Science 1998;279(5348):208–211. [PubMed: 9422689]
4. Shi Kam NW, O'Connell M, Wisdom JA, Dai H. Proceedings of the National Academy of Sciences 2005;102(33):11600–11605.
5. Trentler TJ, Hickman KM, Goel SC, Viano AM, Gibbons PC, Buhro WE. Science 1995;270(5243): 1791–1794.
6. Tuan HY, Lee DC, Hanrath T, Korgel BA. Nano Lett 2005;5(4):681–684. [PubMed: 15826108]
7. Kuno M, Ahmad O, Protasenko V, Bacinello D, Kosel TH. Chem Mater 2006;18(24):5722–5732.

8. Panda AB, Glaspell G, El-Shall MS. J Am Chem Soc 2006;128:2790–2791. [PubMed: 16506744]
9. Saunders AE, Popov I, Banin U. J Phys Chem B 2006;110(50):25421–25429. [PubMed: 17165989]
10. Yong KT, Sahoo Y, Choudhury KR, Swihart MT, Minter JR, Prasad PN. Nano Lett 2006;6(4):709–714. [PubMed: 16608269]
11. Yong KT, Sahoo Y, Choudhury KR, Swihart MT, Minter JR, Prasad PN. Chem Mater 2006;18(25):5965–5972.
12. Yong KT, Sahoo Y, Swihart MT, Prasad PN. J Phys Chem C 2007;111(6):2447–2458.
13. Yong KT, Sahoo Y, Swihart MT, Prasad PN. Adv Mater 2006;18:1978–1982.
14. Yong KT, Sahoo Y, Zeng H, Swihart MT, Minter JR, Prasad PN. Chem Mater 2007;19(17):4108–4110.
15. Kim W, Ng JK, Kunitake ME, Conklin BR, Yang P. J Am Chem Soc 2007;129(23):7228–7229. [PubMed: 17516647]
16. Prasad, PN. Nanophotonics. Wiley-Interscience; New York: 2004.
17. Bierman MJ, Lau YKA, Jin S. Nano Lett 2007;7(9):2907–2912. [PubMed: 17672508]
18. Manna L, Milliron DJ, Meisel A, Scher EC, Alivisatos AP. Nat Mater 2003;2(6):382–385. [PubMed: 12764357]
19. Yin Y, Alivisatos AP. Nature 2005;437(7059):664–670. [PubMed: 16193041]
20. Yong K-T, Sahoo Y, Swihart M, Schneeberger P, Prasad P. Topics in Catalysis 2008;47(1):49–60.
21. Burda C, Chen X, Narayanan R, El-Sayed MA. Chem Rev 2005;105(4):1025–1102. [PubMed: 15826010]
22. Peng ZA, Peng X. J Am Chem Soc 2001;123(1):183–184. [PubMed: 11273619]
23. Peng ZA, Peng X. J Am Chem Soc 2001;123(7):1389–1395.
24. Peng ZA, Peng X. J Am Chem Soc 2002;124(13):3343–3353. [PubMed: 11916419]
25. Talapin DV, Mekis I, Gotzinger S, Kornowski A, Benson O, Weller H. J Phys Chem B 2004;108:18826–18831.
26. Prasad, PN. Biophotonics. Wiley-Interscience; New York: 2004.
27. Huang X, El-Sayed IH, Qian W, El-Sayed MA. J Am Chem Soc 2006;128(6):2115–2120. [PubMed: 16464114]
28. Alivisatos P. Nat Biotech 2004;22(1):47–52.
29. Huynh WU, Dittmer JJ, Alivisatos AP. Science 2002;295(5564):2425–2427. [PubMed: 11923531]
30. Mokari T, Banin U. Chem Mater 2003;15:3955–3960.
31. Peng X, Manna L, Yang W, Wickham J, Scher E, Kadavanich A, Alivisatos AP. Nature 2000;404(6773):59–61. [PubMed: 10716439]
32. Fu A, Gu W, Boussert B, Koski K, Gerion D, Manna L, LeGros M, Larabell CA, Alivisatos AP. Nano Lett 2007;7(1):179–182. [PubMed: 17212460]
33. Yong KT, Qian J, Roy I, Lee HH, Bergey EJ, Tramposch KM, He S, Swihart MT, Maitra A, Prasad PN. Nano Lett 2007;7(3):761–765. [PubMed: 17288490]
34. Dubertret B, Skourides P, Norris DJ, Noireaux V, Brivanlou AH, Libchaber A. Science 2002;298(5599):1759–1762. [PubMed: 12459582]
35. Gil PR, Parak WJ. ACS Nano 2008;2(11):2200–2205. [PubMed: 19206383]
36. Rajangam K, Behanna HA, Hui MJ, Han X, Hulvat JF, Lomasney JW, Stupp SI. Nano Letters 2006;6(9):2086–2090. [PubMed: 16968030]
37. Cheng Z, Wu Y, Xiong Z, Gambhir SS, Chen X. Bioconjugate Chem 2005;16(6):1433–1441.
38. Cai W, Shin DW, Chen K, Gheysens O, Cao Q, Wang SX, Gambhir SS, Chen X. Nano Lett 2006;6(4):669–676. [PubMed: 16608262]
39. Zhou M, Ghosh I. Peptide Science 2007;88(3):325–339. [PubMed: 17167795]
40. Manna L, Scher EC, Li LS, Alivisatos AP. Journal of the American Chemical Society 2002;124(24):7136–7145. [PubMed: 12059239]
41. Feldmann G, Dhara S, Fendrich V, Bedja D, Beaty R, Mullendore M, Karikari C, Alvarez H, Iacobuzio-Donahue C, Jimeno A, Gabrielson KL, Matsui W, Maitra A. Cancer Res 2007;67(5):2187–2196. [PubMed: 17332349]

42. Feldmann G, Fendrich V, McGovern K, Bedja D, Bisht S, Alvarez H, Koorstra JBM, Habbe N, Karikari C, Mullendore M, Gabrielson KL, Sharma R, Matsui W, Maitra A. Mol Cancer Ther 2008;7 (9):2725–2735. [PubMed: 18790753]
43. Soo Choi H, Liu W, Misra P, Tanaka E, Zimmer JP, Itty Ipe B, Bawendi MG, Frangioni JV. Nat Biotech 2007;25(10):1165–1170.
44. Liu W, Choi HS, Zimmer JP, Tanaka E, Frangioni JV, Bawendi M. J Am Chem Soc 2007;129(47): 14530–14531. [PubMed: 17983223]
45. Qian X, Peng XH, Ansari DO, Yin-Goen Q, Chen GZ, Shin DM, Yang L, Young AN, Wang MD, Nie S. Nat Biotech 2008;26(1):83–90.
46. Chen H, Wang Y, Xu J, Ji J, Zhang J, Hu Y, Gu Y. Journal of Fluorescence 2008;18(5):801–811. [PubMed: 18176780]
47. Yong KT. Nanotechnology 2009;20(1):015102.
48. Gao X, Cui Y, Levenson RM, Chung LWK, Nie S. Nat Biotech 2004;22(8):969–976.
49. Akerman ME, Chan WCW, Laakkonen P, Bhatia SN, Ruoslahti E. Proceedings of the National Academy of Sciences 2002;99(20):12617–12621.
50. Yong KT, Roy I, Pudavar HE, Bergey EJ, Tramposch KM, Swihart MT, Prasad PN. Advanced Materials 2008;20(8):1412–1417.
51. Xu G, Yong KT, Roy I, Mahajan SD, Ding H, Schwartz SA, Prasad PN. Bioconjugate Chemistry 2008;19(6):1179–1185. [PubMed: 18473444]
52. Kim S, Lim YT, Soltesz EG, De Grand AM, Lee J, Nakayama A, Parker JA, Mihaljevic T, Laurence RG, Dor DM, Cohn LH, Bawendi MG, Frangioni JV. Nat Biotech 2004;22(1):93–97.
53. Michalet X, Pinaud FF, Bentolila LA, Tsay JM, Doose S, Li JJ, Sundaresan G, Wu AM, Gambhir SS, Weiss S. Science 2005;307(5709):538–544. [PubMed: 15681376]
54. Kim J, Kim KS, Jiang G, Kang H, Kim S, Kim BS, Park MH, Hahn SK. Biopolymers 2008;89(12): 1144–1153. [PubMed: 18690665]
55. Manzoor K, Johny S, Thomas D, Setua S, Menon D, Nair S. Nanotechnology 2009;20(6):065102.
56. Karikari CA, Roy I, Tryggestad E, Feldmann G, Pinilla C, Welsh K, Reed JC, Armour EP, Wong J, Herman J, Rakheja D, Maitra A. Mol Cancer Ther 2007;6(3):957–966. [PubMed: 17339366]

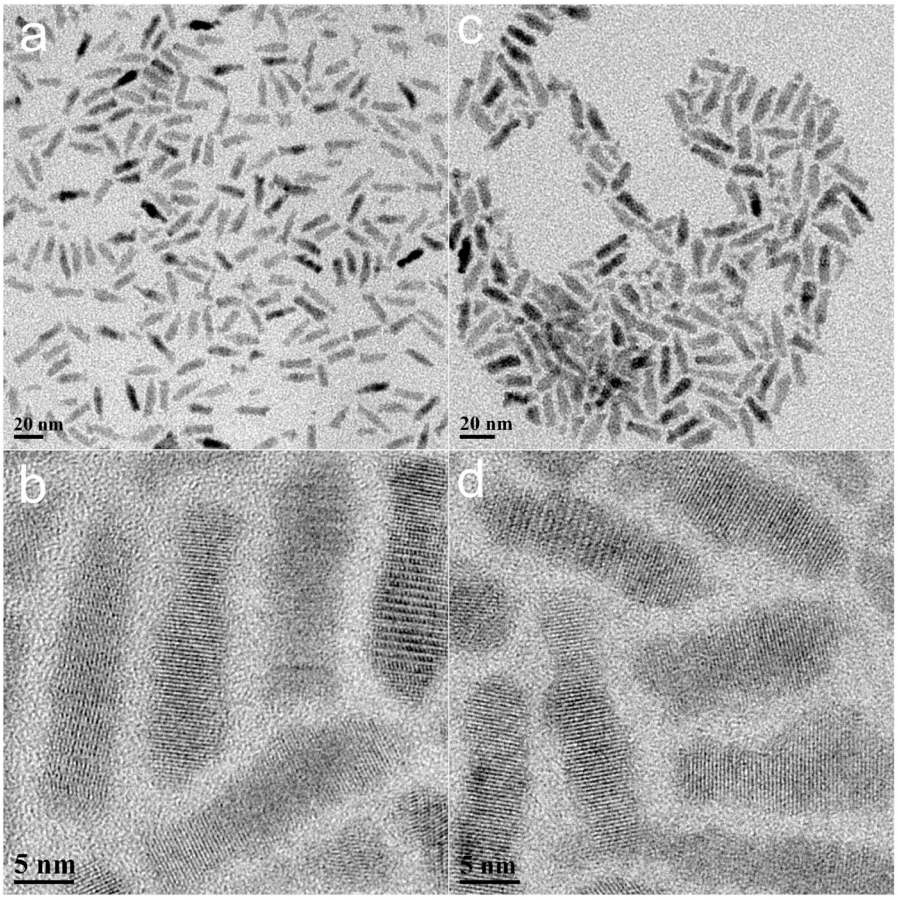

Figure 1.
TEM images of CdSe/CdS/ZnS QRs dispersed in organic (a & b) and aqueous (c & d) media. The average length and diameter of the nanorods are 20.5 and 4.5 nm, respectively. The aspect ratio of the nanorods is 4.5.

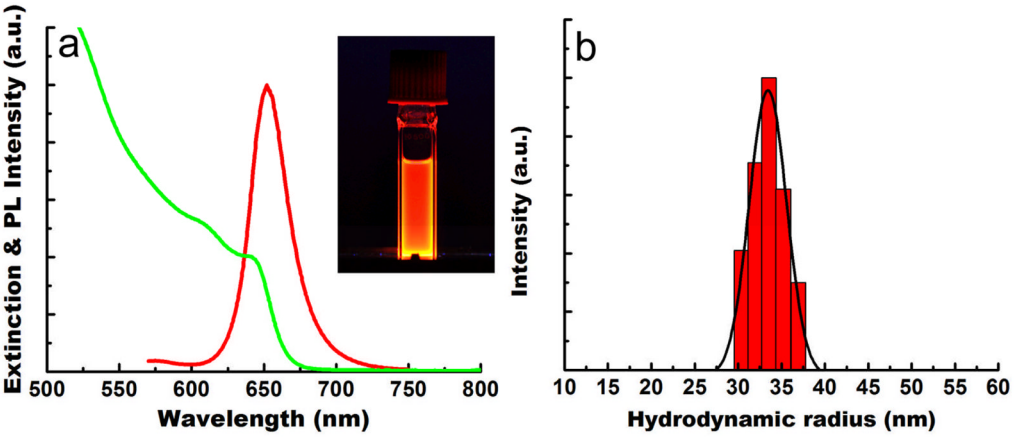

Figure 2.
(a) UV-vis absorption (green) and PL (red) spectra of monodispersed CdSe/CdS/ZnS QRs. (b) DLS plot of monodispersed micelle-encapsulated QRs.

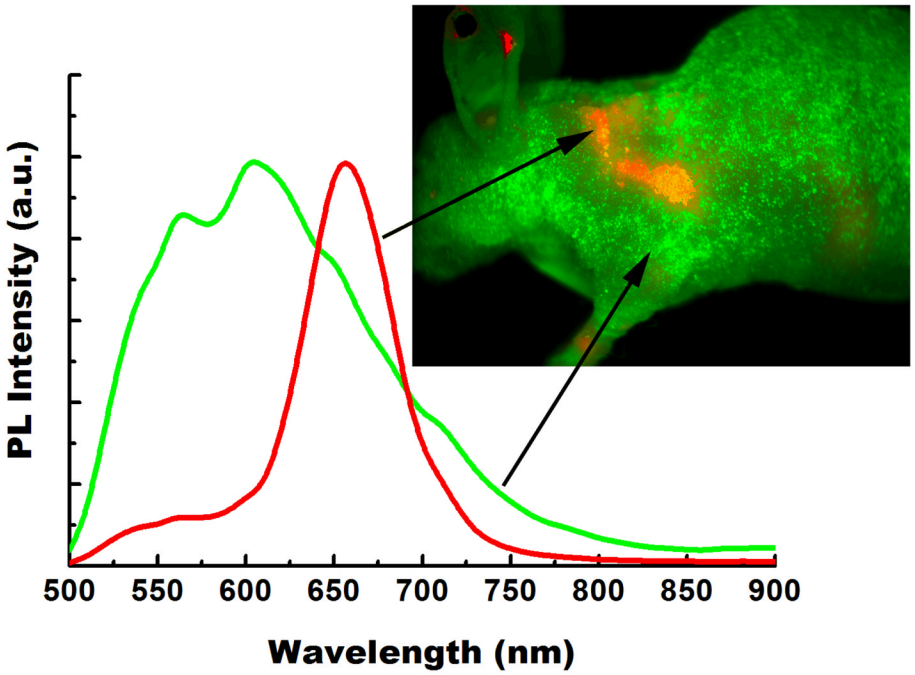

Figure 3.
The unmixing spectra of autofluorescence (green) and QR (red) from a tumor-bearing nude mouse treated with QR bioconjugates. QR spectrum was obtained by subtraction of the autofluorescence signal from the mixture signal of the mouse treated with QR bioconjugates.

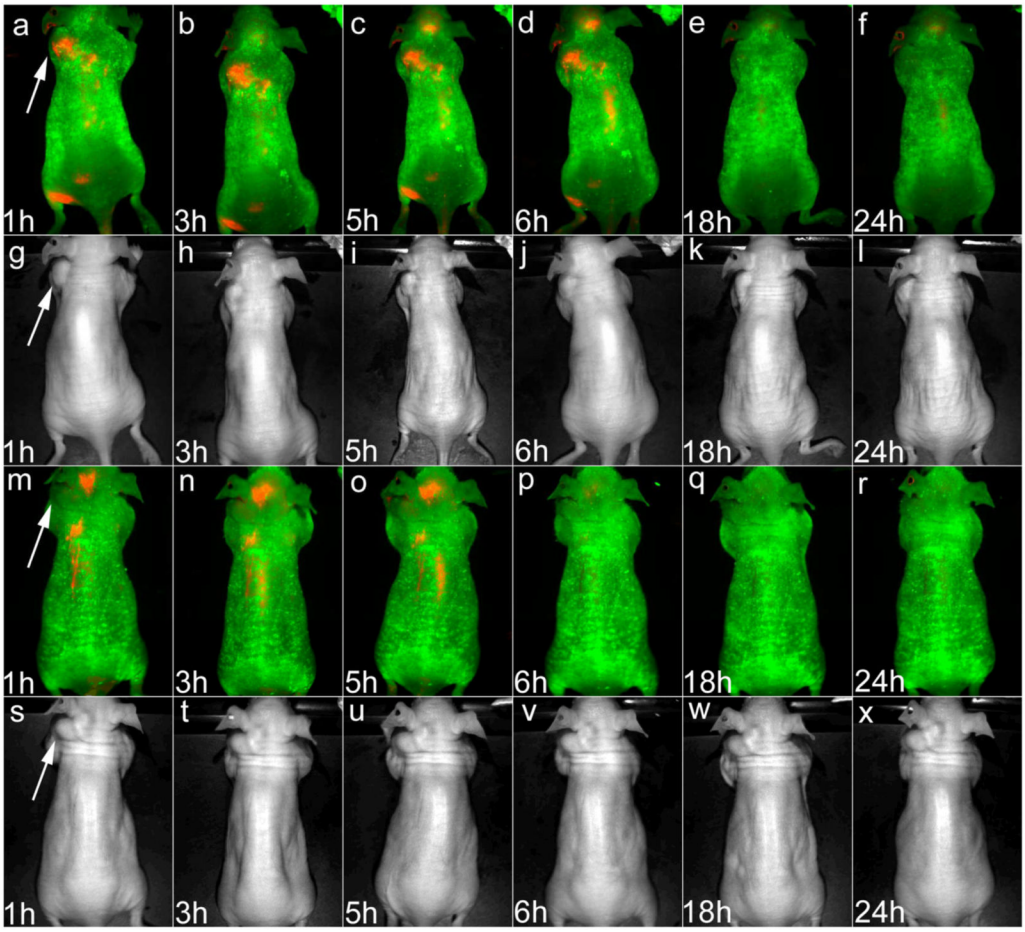

Figure 4.

Time dependent *in vivo* luminescence imaging of Panc-1 tumor-bearing mice (left shoulder, pointed by white arrows) injected with ~1 mg of cRGD-peptide conjugated QRs (panels a–f) and unconjugated QRs (panels m–r), respectively. All images were acquired under the same experimental conditions. The autofluorescence from tumor-bearing mice is coded green color and the unmixed QR signal is coded red color. Prominent uptake in the liver, spleen and lymph nodes was also visible. Transmission images in panels g–i and panels s–x corresponds to the luminescence images in panels a–f and panels m–r, respectively.

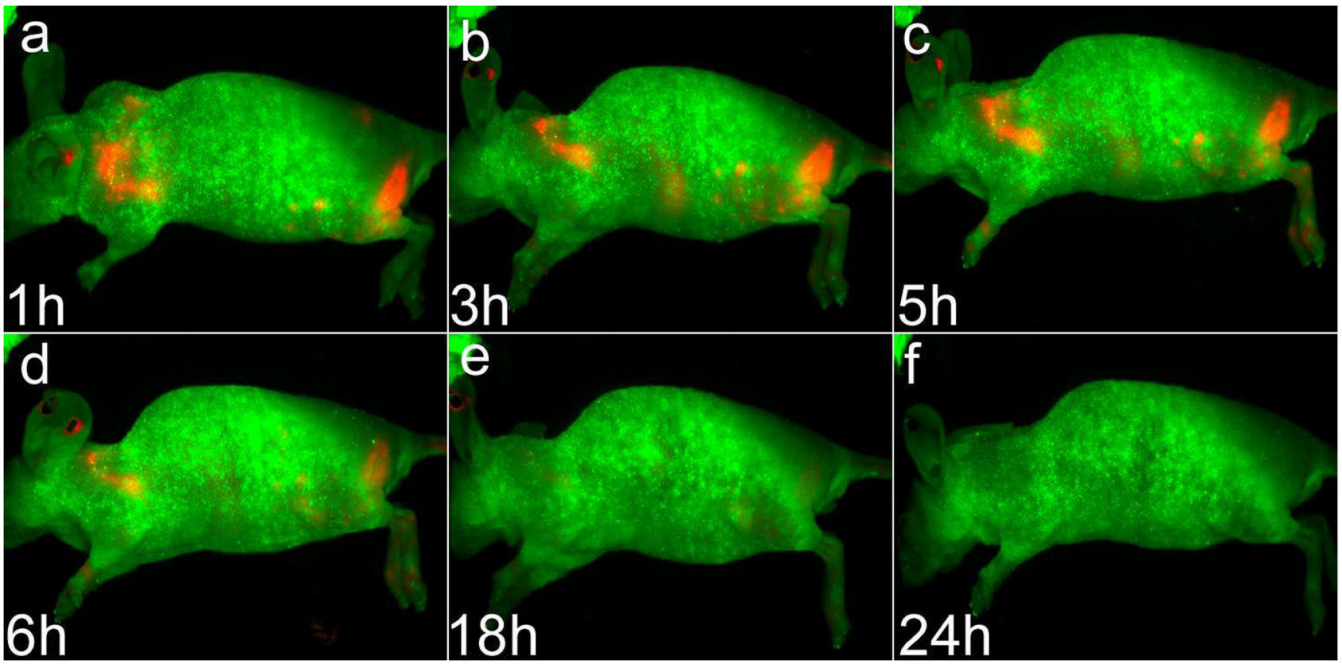

Figure 5.
Lateral view of *in vivo* luminescence imaging of Panc-1 tumor-bearing mice (left shoulder) injected with ~1 mg of cRGD-peptide conjugated QRs. These images correspond to the images taken in Figure 4, panels a–f.

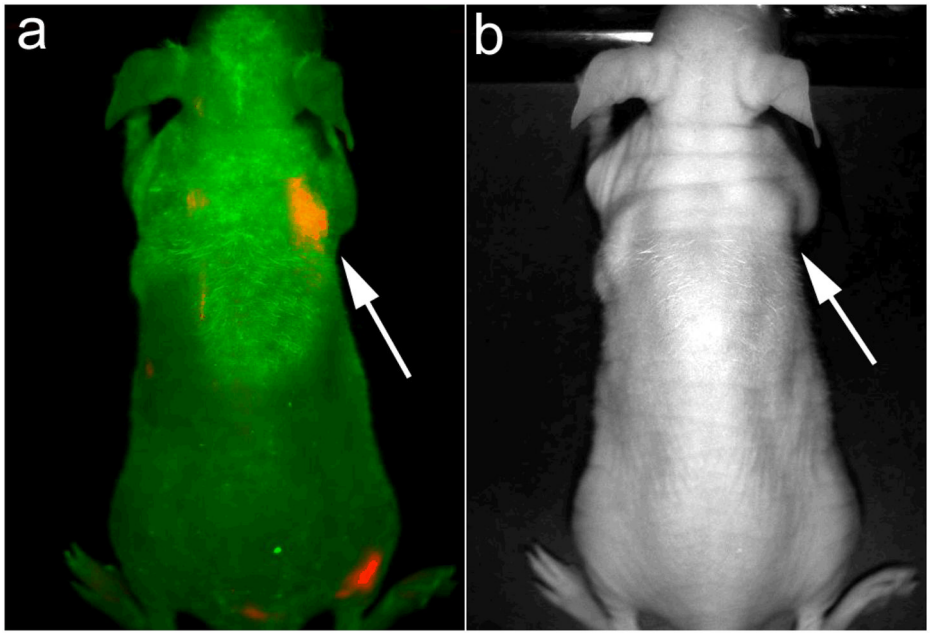

Figure 6.
In vivo luminescence imaging of mice at 2 weeks post-inoculation of Panc-1 cancer cells subcutaneously (right shoulder, pointed by white arrows) injected with ~0.5 mg of cRGD-peptide conjugated QRs. The autofluorescence from tumor-bearing mice is coded green color and the unmixed QR signal is coded red color. Transmission image in Figure 6b corresponds to the luminescence image in Figure 6a.

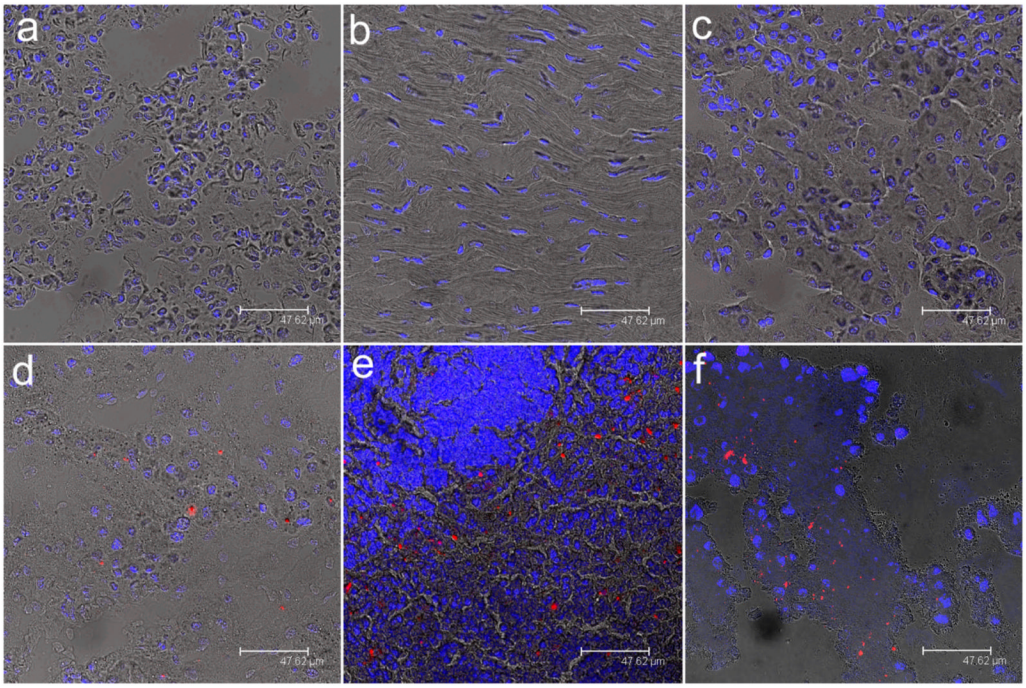

Figure 7.
Tissue sections from Panc-1 tumor-bearing mice intravenously injected with cRGD peptide-conjugated CdSe/CdS/ZnS QRs. Tissues were harvested from lung (a), heart (b), kidney (c), liver (d), spleen (e), and tumor (f). In all cases, blue represents emission from Hoechst 33342 and red represents emission from functionalized CdSe/CdS/ZnS QRs.

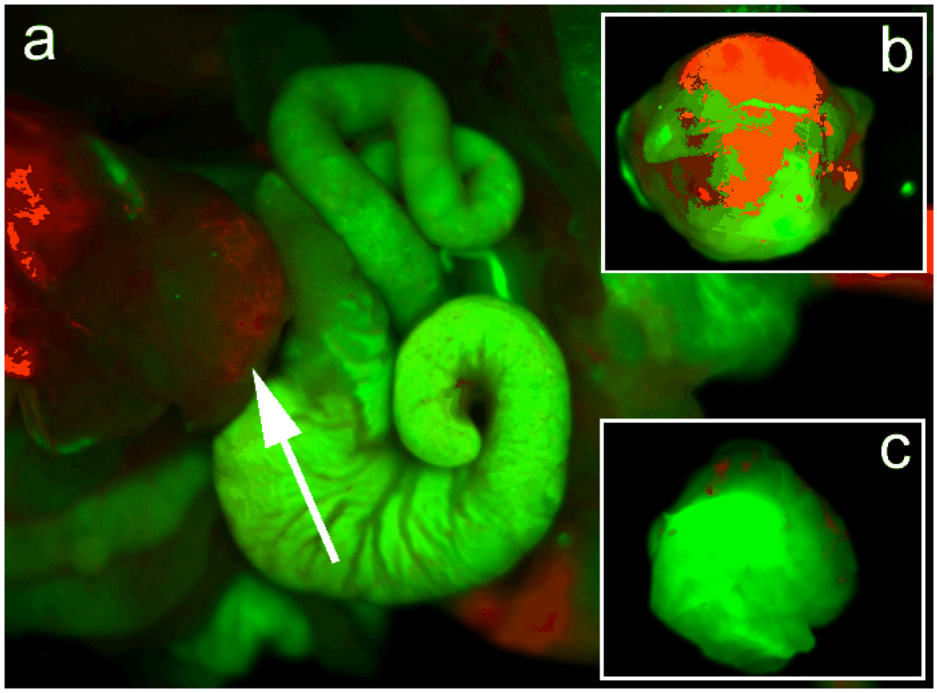

Figure 8.
(a) *In vivo* luminescence imaging of orthotopic tumor model mouse (tumor is pointed by white arrow) injected with ~1 mg of cRGD-peptide conjugated QRs. The autofluorescence from mice is coded green color and the unmixed QR signal is coded red color. (b) Ex vivo orthotopic tumor luminescent images of unconjugated QRs and (c) cRGD conjugated QRs harvested from mice at 2 hours, postinjection. The autofluorescence from tumor is coded green color and the unmixed QR signal is coded red color.

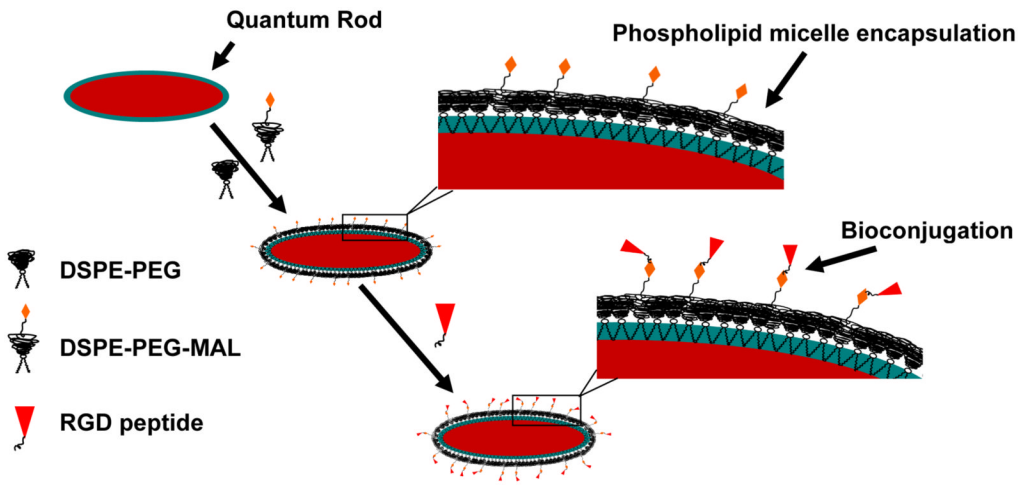

Scheme 1.
Schematic illustration showing the formation of the water-dispersible CdSe/CdS/ZnS QR-bioconjugates.